Effect of Ru–Mn redox interactions on the hole carrier density in pulsed electron deposited $La_{1-x}Pb_xMn_{0.8}Ru_{0.2}O_3$ ($0.2 \leq x \leq 0.4$) thin films

2008 J. Phys.: Condens. Matter 20 235205

(http://iopscience.iop.org/0953-8984/20/23/235205)

J. Phys.: Condens. Matter **20** (2008) 235205 (7pp) doi:10.1088/0953-8984/20/23/235205

Effect of Ru–Mn redox interactions on the hole carrier density in pulsed electron deposited $La_{1-x}Pb_xMn_{0.8}Ru_{0.2}O_3$ ($0.2 \leqslant x \leqslant 0.4$) thin films

S Sundar Manoharan[1,4], Brajendra Singh[1], Ranjan K Sahu[2], A Zimmer[3], S-H Lim[3], L G Salamanca-Riba[3] and V Chandra[1]

[1] Materials Chemistry Laboratory, Indian Institute of Technology Kanpur, Kanpur-208016, India
[2] National Metallurgical Laboratory, Jamshedpur 831 007, India
[3] Center for Superconductivity and, Department of Materials Science and Engineering, University of Maryland, MD 20742-4111, USA

E-mail: ssundar@iitk.ac.in

Received 7 December 2007, in final form 20 March 2008
Published 30 April 2008
Online at stacks.iop.org/JPhysCM/20/235205

Abstract

Pulsed electron deposited thin films of Ru substituted $La_{1-x}Pb_xMn_{0.8}Ru_{0.2}O_3$ ($0.2 \leqslant x \leqslant 0.4$) show an increase in the magneto-resistance ratio by ~5–15% at the respective metal to insulator transition (T_{MIT}) temperature when compared to the parent $La_{0.6}Pb_{0.4}MnO_3$ thin film. A systematic decrease in T_{MIT} is observed from ~310 to ~260 K when the hole (Pb) concentration varies from 40 to 20% with constant 20% Ru substitution at the Mn site. The x-ray rocking curve and high-resolution transmission electron microscopy (HRTEM) images of the thin films suggest that Ru occupies the Mn site and shows epitaxial growth of the films on the $LaAlO_3$ (LAO) substrate. Transport and magneto-resistive properties show that Ru substitution maintains a considerable hole carrier density (due to Mn^{4+}:$t_{2g}^3e_g^0$/Ru^{5+}:$t_{2g}^3e_g^0$) even for $La_{0.8}Pb_{0.2}Mn_{0.8}Ru_{0.2}O_3$ (8282) composition, which influences the double exchange interactions.

1. Introduction

Colossal magneto-resistive manganites show a large decrease in resistance in the presence of applied magnetic field due to the interactions between the $Mn^{+3}(t_{2g}^3e_g^1)/Mn^{+4}(t_{2g}^3e_g^0)$ redox couple via the O atom in the Mn–O–Mn lattice [1, 2]. The resistance and the magneto-resistance (MR) behavior stem from the interplay of Jahn–Teller distortion, the strength of the Zener double exchange interaction, super-exchange and coulombic interactions; which can be controlled by the concentration of $Mn^{+3}(t_{2g}^3e_g^1)$ and $Mn^{4+}(t_{2g}^3e_g^0)$ valence states, which essentially changes the hole carrier density in the Mn–O–Mn sublattice [3–5].

Polycrystalline manganites show MR properties at Curie temperature (T_C) due to the intrinsic effects and dominant extrinsic interactions at low temperatures, while in thin films intrinsic interactions dominate, ignoring the grain boundary and phase separation effects [6]. Although thin films of $La_{0.7}Ca_{0.3}MnO_3$ show large MR at T_C (260 K), many other candidates show room temperature MR i.e. $La_{0.7}Sr_{0.3}MnO_3$ (−35%), $La_{0.7}Ba_{0.3}MnO_3$ (−60%) and $La_{0.6}Pb_{0.4}MnO_3$ (−40%) [1, 7–9]. In addition, the Mn-site substituted Ru doped $La_{0.7}Pb_{0.3}Mn_{1-x}Ru_xO_3$ perovskite series show dominant Zener double exchange mediated transport [10]. The novelty in this substitution lies in the fact that the Ru–Mn redox interactions provide another redox pair $Mn^{+3}(t_{2g}^3e_g^1)/Ru^{5+}(t_{2g}^3e_g^0)$, in addition to $Mn^{3+}(t_{2g}^3e_g^1)/Mn^{4+}(t_{2g}^3e_g^0)$, where Ru^{5+} (due to iso-electronic similarity) works similarly to Mn^{4+} and provides holes in the manganites [10]. The role of Ru–Mn redox interactions is further exemplified in the melting of the charge ordering

[4] Author to whom any correspondence should be addressed.

in manganites, the increase in magnetic moment, the enhancement of the Curie temperature and the T_{MIT} transition of layered manganites, magnetic pair making, and breaking effects [11–15]. Further, in ruthenates, an increase in the magneto-resistive behavior is found due to the presence of Mn^{3+}/Mn^{4+} and Ru^{4+}/Ru^{5+} redox pairs [16]. Here we show the magneto-resistive studies in Ru substituted $La_{1-x}Pb_xMn_{0.8}Ru_{0.2}O_3$ ($0.2 \leqslant x \leqslant 0.4$) thin films where the Ru doping level is kept constant (20%) while varying the hole carrier concentration at the A site; Pb content varying from 40% to 20%.

We have employed the pulsed electron deposition (PED) method, which is an ablation based thin film growth technique [17]. In addition, the thermodynamic properties of the target material such as melting point and specific heat become unimportant for the evaporation process in PED, particularly advantageous in the case of complex, multi-component oxides such as $YaBa_2Cu_3O_7$, wide band gap materials (SiO_2) etc [17–19]. $La_{0.6}Pb_{0.4}MnO_3$ and $La_{1-x}Pb_xMn_{0.8}Ru_{0.2}O_3$ ($0.2 \leqslant x \leqslant 0.4$) can serve as reference systems to study the Ru–Mn redox interactions on the hole carrier density in PED deposited thin films for the following reasons; $La_{0.6}Pb_{0.4}MnO_3$ exhibits Curie temperature (T_C), metal to insulator transition temperature (T_{MIT}), and large MR ratio at room temperature [9]. In this study, Ru substituted compositions show increased MR compare to $La_{0.6}Pb_{0.4}MnO_3$ thin film and the $La_{0.8}Pb_{0.2}Mn_{0.8}Ru_{0.2}O_3$ (8282) composition shows substantial T_C and MR ratio due to the hole carrier density being influenced by the presence of Ru–Mn redox interactions. Thus it is envisaged that we should highlight the possible influence of Ru in maintaining the hole carrier density in this series.

2. Experimental details

Bulk $La_{1-x}Pb_xMn_{0.8}Ru_{0.2}O_3$ ($0.2 \leqslant x \leqslant 0.4$) and $La_{0.6}Pb_{0.4}MnO_3$ samples were prepared by the solid state reaction method. Stoichiometric amounts of La_2O_3, $(PbCO_3)_2{\cdot}Pb(OH)_2$, MnO_2, and RuO_2 were mixed and calcined at 900 °C for 24 h in air. The calcined powders were palletized to 20 mm diameter pellets, which were going to be used as targets to deposit thin films, followed by sintering at 1050 °C for 48 h. Thin films of $La_{0.6}Pb_{0.4}MnO_3$ and $La_{1-x}Pb_xMn_{0.8}Ru_{0.2}O_3$ ($0.2 \leqslant x \leqslant 0.4$) were grown on (001) $LaAlO_3$ (LAO) substrate using the PED method by keeping the substrate temperature, T_s, ~650 °C. In the PED process, the pulsed electron beam source operates between 10 and 20 kV with 1–10 Hz repetition rate. The beam duration was 100 ns with pulsed beam energy in the range of 0.2–0.8 J. During deposition, the chamber pressure was maintained at 13 mTorr (1.73 Pa) of O_2 pressure. After the deposition, all the films were annealed *in situ* at 650 °C and 670 °C for 45 min. During annealing, the chamber pressure was kept constant at 400 mTorr (53.32 Pa) and 400 Torr (53328 Pa) of O_2 pressure. The target to substrate distance for all the depositions was optimized to be ~9.5 cm. Structural and micro-structural properties of the samples were characterized by x-ray diffraction and high-resolution transmission electron microscopy (HRTEM). Compositional analysis of the PED deposited thin films was done using the Rutherford backscattering method (RBS). Careful analyses of the films grown in the required conditions do show nearly exact composition within 3–5% error. Resistance and magneto-resistive properties of the films were measured using a Quantum Design PPMS instrument. The negative MR ratio is defined as $\Delta R/R = [R_H - R_0]/R_0$, where R_0 and R_H are the resistances without and with magnetic field, respectively.

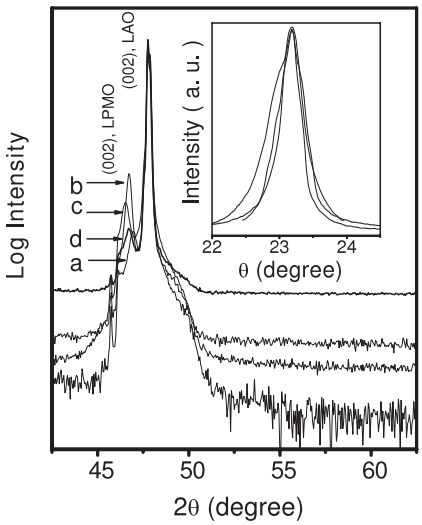

Figure 1. X-ray diffraction pattern (θ–2θ scans) for (a) $La_{0.6}Pb_{0.4}MnO_3$ and $La_{1-x}Pb_xMn_{0.8}Ru_{0.2}O_3$, where (b) $x = 0.4$, (c) $x = 0.3$, and (d) $x = 0.2$ thin films on the (001) LAO substrate. The inset shows the rocking curve for the (002) peak. Rocking curve analysis shows textured films of $La_{1-x}Pb_xMn_{0.8}Ru_{0.2}O_3$, where $x = 0.2$, 0.3, and 0.4, on an LAO substrate.

3. Results

The log intensity plots of x-ray diffraction patterns for the films deposited at 18 kV source voltage and 7 Hz repetition rate indicate that *c*-axis oriented epitaxial films grow with ease on a (001) LAO substrate. Figure 1 shows the XRD pattern of the $La_{0.6}Pb_{0.4}MnO_3$ and $La_{1-x}Pb_xMn_{0.8}Ru_{0.2}O_3$ thin films, where $x = 0.2$, 0.3 and 0.4. From the (002) peak, we obtain the lattice parameter $c = 3.867$ Å for $La_{0.6}Pb_{0.4}MnO_3$. This matches well with the reported value in the literature. However, the lattice parameter increases from 3.867 to 3.899 Å with 20% of Ru substituted at the Mn site. The presence of Ru^{4+} (0.62 Å) and especially Ru^{5+} (0.56 Å) increases the Mn^{3+} (0.65 Å) concentration, accordingly the lattice expands as found in Ru doped $La_{0.7}Ca_{0.3}Mn_{1-x}Ru_xO_3$ thin films [20]. The increase in lattice parameter suggests that Ru occupies the Mn site of the perovskite structure, due to its crystal field stabilization energy which favors octahedral site occupancy. The FWHM of the rocking curves along the (002) peak in $La_{1-x}Pb_xMn_{0.8}Ru_{0.2}O_3$ thin films is found to be close to 0.5° (inset to figure 1) in Ru substituted films.

In figure 2, we show the cross-sectional high-resolution TEM micrograph of $La_{0.6}Pb_{0.4}Mn_{0.8}Ru_{0.2}O_3$ film on an LAO substrate. Figure 2(a) shows a low magnification bright

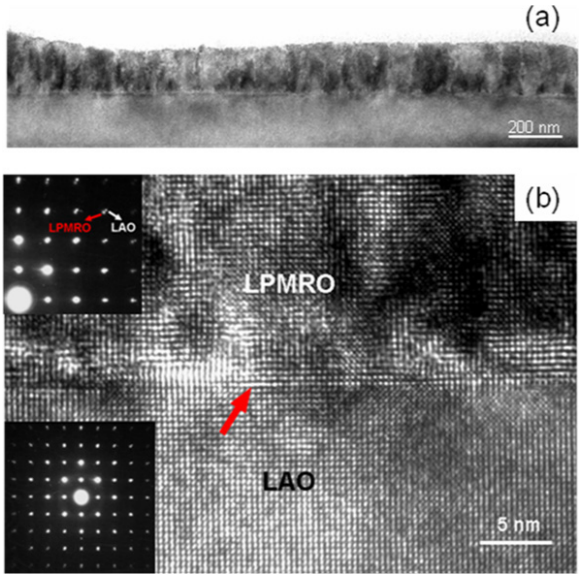

Figure 2. HRTEM images of $La_{0.6}Pb_{0.4}Mn_{0.8}Ru_{0.2}O_3$ thin film deposited on LAO substrate. (a) Low magnification bright field image of $La_{0.6}Pb_{0.4}Mn_{0.8}Ru_{0.2}O_3$ thin film deposited on LAO substrate. (b) The interface between LAO and $La_{0.6}Pb_{0.4}Mn_{0.8}Ru_{0.2}O_3$ film is shown with an arrow. The inset shows a selected area diffraction pattern, confirming good epitaxial growth.

field image of a $La_{0.6}Pb_{0.4}Mn_{0.8}Ru_{0.2}O_3$ thin film on an LAO substrate. The figure shows that the film is single crystalline with no impurities or defects in the whole thin area of the sample. In figure 2(b), the arrow shows a sharp interface between the film and the substrate with no evidence for any secondary phase. The image shows good epitaxial growth. The inset to figure 2 shows the diffraction pattern of interface and substrate, further substantiating the epitaxial growth and the crystallinity of our films. Though we do not apparently observe any splitting for the [001] spot, a small splitting of the [004] spot gives a clue to the close lattice parameter matching between the substrate and the film, 3.789 Å and 3.899 Å respectively. The lattice mismatch between $La_{0.6}Pb_{0.4}Mn_{0.8}Ru_{0.2}O_3$ thin film and $LaAlO_3$ substrate is found (−2.9%), which is quite substantial when compared to the growth of manganites on STO substrate (0.91%) [20]. Such a large mismatch eventually leads to stress and defect formation in order to partially relax the in-plane tensile strain, which ultimately affects the T_{MIT} in manganites. However, to avoid the effect of tensile strain on the transport properties of manganite, we have deposited ∼2000 Å thick films.

Figure 3(a) shows the resistance versus temperature plot of $La_{0.6}Pb_{0.4}MnO_3$ and $La_{0.6}Pb_{0.4}Mn_{0.8}Ru_{0.2}O_3$ thin films. Leung *et al* have shown the magnetic transition temperature for the single crystal of $La_{0.69}Pb_{0.31}MnO_3$ ∼337 K, while pulsed laser deposited (PLD) $La_{0.6}Pb_{0.4}MnO_3$ thin film exhibits T_{MIT} ∼ 300 K [9]. It is found that PED deposited $La_{0.6}Pb_{0.4}MnO_3$ thin film exhibits T_{MIT} above 310 K (figure 3(a)) which confirms that the PED retains the stoichiometry in the thin films; a nominal decrease in T_{MIT} is found due to the lattice mismatch between the substrate and the $La_{0.6}Pb_{0.4}MnO_3$ thin film (−2.9%) compared to bulk samples. However, our

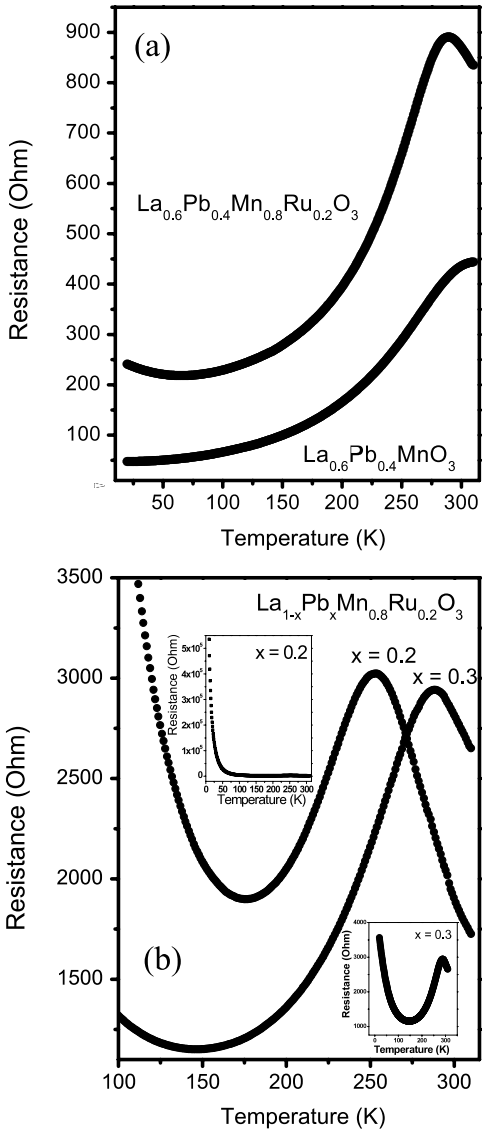

Figure 3. (a) and (b) Plot of resistance as a function of temperature for the $La_{0.6}Pb_{0.4}MnO_3$ and $La_{1-x}Pb_xMn_{0.8}Ru_{0.2}O_3$ ($0.2 \leqslant x \leqslant 0.4$) thin films. 20% Pb doped film shows T_{MIT} ∼ 250 K with 20% Ru substitution at the Mn site. Inset to (b) shows the resistance versus temperature data in the temperature range 10–300 K.

$La_{0.6}Pb_{0.4}Mn_{0.8}Ru_{0.2}O_3$ thin film shows the transition peak with T_{MIT} ∼ 290 K. The difference between the T_{MIT} of $La_{0.6}Pb_{0.4}MnO_3$ and $La_{0.6}Pb_{0.4}Mn_{0.8}Ru_{0.2}O_3$ observed is ∼15 K with a nominal increase in resistance around T_{MIT}, which shows that Ru doping provides holes in the Mn–O–Ru basal plane and participates in long range ordering and favors double exchange mediated transport. To evaluate the sustenance of the hole carrier density, we have kept the Ru doping at the Mn site constant and have varied the Pb content at the A site. In all the compositions a close match between the T_C and T_{MIT} is observed justifying the magnetic ordering, and transport is mediated via Zener's double exchange model [4]. Figure 3(b) shows the resistance versus temperature plot of $La_{0.7}Pb_{0.3}Mn_{0.8}Ru_{0.2}O_3$ (7382) and $La_{0.8}Pb_{0.2}Mn_{0.8}Ru_{0.2}O_3$ (8282) films. The PED deposited thin films of (7382) and (8282) compositions exhibit

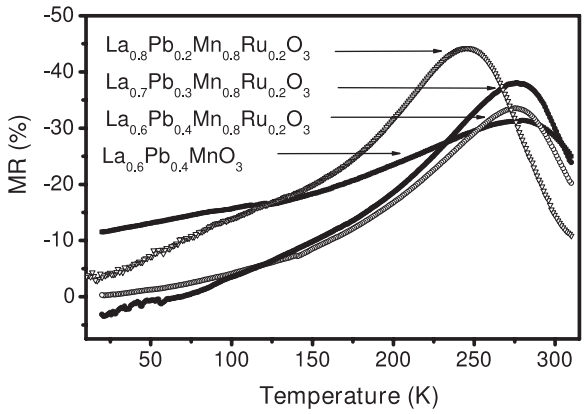

Figure 4. Plot of MR ($H = 5$ T) as a function of temperature for $La_{0.6}Pb_{0.4}MnO_3$ and $La_{1-x}Pb_xMn_{0.8}Ru_{0.2}O_3$, where $x = 0.4$, 0.3, and 0.2.

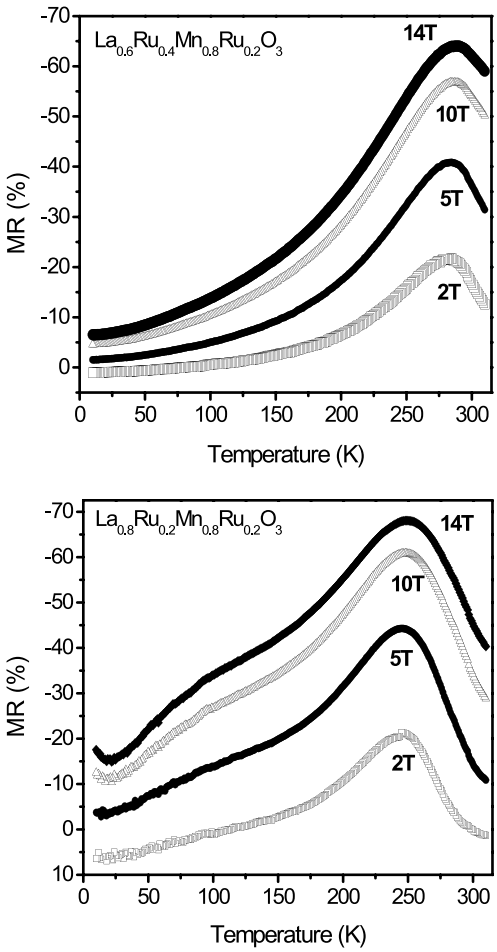

Figure 5. MR as a function of magnetic field for $La_{0.6}Pb_{0.4}Mn_{0.8}Ru_{0.2}O_3$ and $La_{0.8}Pb_{0.2}Mn_{0.8}Ru_{0.2}O_3$ in the temperature range 20–310 K. Note the increased MR in the Ru doped film compare to $La_{0.6}Pb_{0.4}MnO_3$ and the presence of positive MR in $La_{0.7}Pb_{0.3}Mn_{0.8}Ru_{0.2}O_3$ thin film.

T_{MIT} at 270 K and 260 K respectively; single crystals of $La_{0.7}Pb_{0.3}MnO_3$ and $La_{0.74}Pb_{0.26}MnO_3$ show magnetic transition at ∼337 and 328 K. It is found that the depth of the resistivity minima and the shifting in the resistivity minima at low temperatures in the $La_{0.7}Pb_{0.3}Mn_{0.8}Ru_{0.2}O_3$ (7382) and $La_{0.8}Pb_{0.2}Mn_{0.8}Ru_{0.2}O_3$ (8282) films increases with decreasing Pb content. Low temperature increase in resistance may arise from charge carrier localization effects, enhanced electron–electron (e–e) interactions (Coulombic interactions, CI effect), disorder from the orbital degrees of freedom, and further antiferromagnetic interactions (suggested by the Goodenough–Kanamori–Anderson (GKA) rule—similar ions couple antiferromagnetically and different ions couple ferromagnetically) due to different redox pairs, namely Mn^{4+}–Mn^{4+}, Ru^{4+}–Ru^{4+}, and Mn^{3+}–Mn^{3+} which cannot be ignored at low temperatures [21, 22]. A systematic change in the transport properties by varying the Pb content in the system matches with the result of $La_{1-x}Sr_xMnO_3$ [23]. Despite a 20% doping of Ru at the Mn site in all the Pb doped manganites, the fact that we still observe substantial T_{MIT} and a delayed upturn in resistivity for a 20% Pb doped manganite $La_{0.8}Pb_{0.2}Mn_{0.8}Ru_{0.2}O_3$ suggests a magnetic pair making effect of Ru along with Mn in the Mn–O–Ru basal plane [15]. It is well understood that an optimum of ∼33% Pb doping is suggested for a dominant Zener double exchange coupling to operate over the super-exchange mediated antiferromagnetic ordering [9]. The result in this series suggests that a cooperative mechanism between Ru and Mn is operative to maintain the hole carrier density.

The magneto-resistance behavior as a function of temperature and applied magnetic fields has been a useful tool to understand the influence of intrinsic (hole) and extrinsic (grain boundary) effects on the magnetic and electronic properties of manganites [24, 25]. A sharp drop in the resistance and the large MR ratio at low temperature and at low magnetic fields have been attributed to the grain boundary effects or to spin glass effect, while linear behavior with the fields near the metal–insulator transition temperature has been modeled based on the magnetic polaron which is a dominant feature in our studies. The MR ratio of $La_{0.6}Pb_{0.4}MnO_3$ and $La_{1-x}Pb_xMn_{0.8}Ru_{0.2}O_3$ thin films at different temperatures between 20 and 300 K and field $H = 5$ T is shown in figure 4. It is seen that MR increases up to −44% for the (8282) composition near to T_{MIT} while it has been found ∼ −70% at 14 T applied magnetic field in figure 5, which further certifies the redox interactions between Mn^{3+}/Mn^{4+} and Ru^{+4}/Ru^{5+} redox pairs [10]. The low temperature MR decreases and the transition peaks become sharp; indicating that the phase separation does not dominate. This feature is completely different from the two distinct T_{MIT} maxima observed with large low temperature MR for Ru doped $La_{0.66}Ca_{0.33}MnO_3$ [26].

The MR ratios of $La_{0.6}Pb_{0.4}MnO_3$ and $La_{1-x}Pb_xMn_{0.8}Ru_{0.2}O_3$ thin films with varying magnetic field from −5 to +5 T at 310 and 20 K are shown in figure 6. Interestingly, the MR ratio increased in the Ru doped films, as shown in figure 6(a) compared to the $La_{0.6}Pb_{0.4}MnO_3$ at 310 K. The MR ratio measured at 20 K shows the signature of positive MR in the Ru doped films as shown in figure 6(b). $La_{0.7}Pb_{0.3}Mn_{0.8}Ru_{0.2}O_3$ film shows a measure of 3% positive MR, which exists up to 5 T applied field

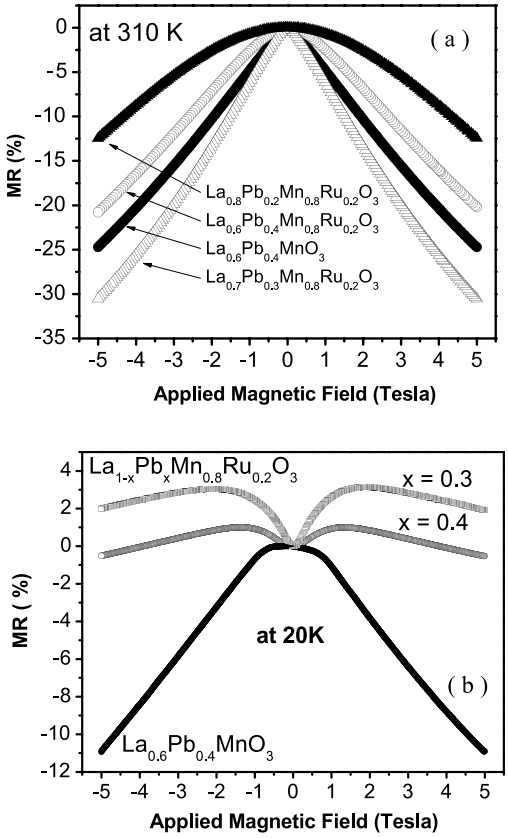

Figure 6. The field dependent MR plot for $La_{1-x}Pb_xMn_{0.8}Ru_{0.2}O_3$ ($0.2 \leqslant x \leqslant 0.4$) thin films at 310 and 20 K.

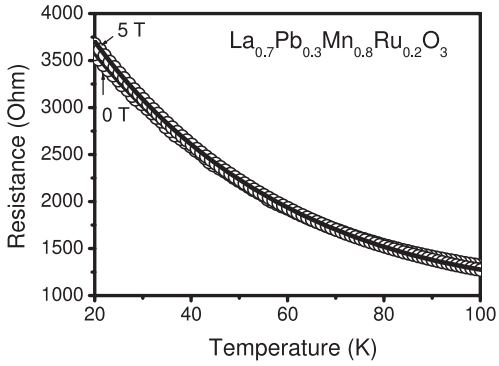

Figure 7. Plot of resistance as a function of temperature (for $T < 100$ K) measured under 0 and 5 T magnetic field for $La_{0.7}Pb_{0.3}Mn_{0.8}Ru_{0.2}O_3$ thin film. The symbols are the experimental data and the solid curves are the theoretical fits.

while $La_{0.6}Pb_{0.4}Mn_{0.8}Ru_{0.2}O_3$ film shows the measure of 1% positive MR. The origin of positive MR due to the quantum interference effects from coulomb interactions between carriers enhanced by disorder has been reported in ferromagnet $Fe_{1-y}Co_ySi$ and in single crystals of $La_{0.7}Pb_{0.3}MnO_3$ between 4.2 and 50 K [27, 28].

In manganites, the resistivity behavior at different temperatures below T_c is well studied and correlated to three dominant effects namely: electron–electron interaction below $T < 50$ K, electron–phonon interaction at 50 K $< T < 0.6T_c$, and to the electron–magnon effects near T_c, where $d\rho/dT < 0$ [29]. However, the ρ versus T curve for Ru doped compositions could not be fitted to the equation $R = R_0 + R_2T^2 + R_{4.5}T^{4.5}$ due to the existence of an upturn in the R versus T curve below 50 K (figure 7); R_0. R_2, and $R_{4.5}$ correspond to the residual resistance, electron–phonon interactions and electron–magnon interactions. In order to fit the data we have added a $T^{1/2}$ term, giving $R = R_0 + R_2T^2 + R_{4.5}T^{4.5} + aT^{1/2}$, which corresponds to electron–electron interactions [24, 29]. As shown in figure 7, the theoretical fits to low temperature resistance measured at $H = 0$ and 5 T for Ru substituted thin film reveal an excellent agreement between the experimental data and theoretical assumptions. Here, the additional term $T^{1/2}$ can be attributed to the Coulomb interaction between the carriers strongly enhanced by disorder. We have found the coefficient of $T^{1/2}$ $(-)625.91$ in the absence of magnetic field which increased to $(-)693.748$ when compared with data collected in the presence of magnetic field 5 T. Therefore, the resistivity below $T < T_c$, due to electron–phonon scattering and electron–magnon scattering, together with a $T^{1/2}$ dependence arising from the disorder-induced Coulomb interaction are responsible for the positive MR in Ru doped thin films. Such a term has been observed in disordered metallic systems, where its coefficient was found to change sign as a function of disorder [24].

4. Discussion

Observation of the systematic decrease in metal to insulator transition (T_{MIT}) from ∼310 to ∼260 K when hole (Pb) concentration varies from 40 to 20% with constant 20% Ru substitution at Mn sites shows that the Ru substitution provides the hole carrier concentration in the Ru–O–Mn basal plane. X-ray absorption spectroscopic studies on bulk samples of $La_{0.6}Pb_{0.4}Mn_{1-x}Ru_xO_3$ show the existence of the redox ionic pairs Mn^{3+}–Ru^{5+} ↔ Ru^{4+}–Mn^{4+} up to $x = 0.2$ and the predominant existence of the single valence ionic state of Mn^{3+} and Ru^{4+} for the higher Ru doped compositions [10]. We have analyzed the effect of Ru doping on the hole carrier density by keeping Ru concentration at 20%, while varying only the Pb content. The contribution to hole carrier density coming from the [Mn^{4+}: ($t_{2g}^3e_g^0$)] concentration appears to be ably augmented by the presence of [Ru^{5+}: $t_{2g}^3e_g^0$] centers which are iso-orbital and iso-electronic to each other [10]. This existence of mixed valence states in the Ru doped compositions could be due to the comparable oxidation and reduction potential of $Mn^{3+} \leftrightarrow Mn^{4+}$ (1.02 eV) and $Ru^{4+} \leftrightarrow Ru^{5+}$ (1.07 eV). Due to the presence of Ru^{5+}, the itinerant e_g electron of Mn^{3+} could be delocalized to the Ru^{5+} center via O:2p orbitals as in the case of Mn^{3+}–O–Mn^{4+}. Ru–Mn redox interactions are also dominant in the manganese doped ruthenate $SrRu_{1-x}Mn_xO_3$, where induced double exchange (DE) is found due to the presence of Mn^{3+}/Mn^{4+} ↔ Ru^{4+}/Ru^{5+} redox ionic pairs, which resulted in the increase in the MR in the bulk sample of $SrRu_{0.5}Mn_{0.5}O_3$ [16]. Recently it has been observed that Ru–Mn redox interactions increase the magnetic moment and conductivity in the non-perovskite

ruthenate $Sr_{4-x}La_xRu_{2-x}Mn_xO_9$ due to the presence of redox pairs Mn^{3+} and Ru^{5+}/Ru^{6+} [30]. It is therefore noteworthy that even for nominal 20% 'A' site doping such as the $La_{0.8}Pb_{0.2}Mn_{0.8}Ru_{0.2}O_3$ (8282) composition, where 20% Ru doped at an Mn site which has 20% Mn^{4+} concentration shows a metal insulator transition at ∼260 K, confirms that the role of Ru is to provide the hole carrier concentration in the Ru–O–Mn basal plane.

Ru substituted compositions show a low temperature increase in the resistance and especially $La_{0.7}Pb_{0.3}Mn_{0.8}Ru_{0.2}O_3$ (7382) film shows positive MR in the presence of 0–5 T applied magnetic field, which is similar to that observed earlier in $La_{0.7}Pb_{0.3}MnO_3$ single crystals. Chen *et al* has shown that the positive MR originated because of quantum interference effects (QIE) and the dependence of resistance on the $T^{1/2}$ coefficient of temperature shows that the Coulombic interactions are dominant in the $La_{0.7}Pb_{0.3}MnO_3$ single crystals at low temperatures [28]. There are three factors involved which contribute to the low temperature increase in resistance. The first one is the non-magnetic randomness induced by doping and defects which results in random potential fluctuations experienced by the e_g electron [31]. The second factor is the disorder from the orbital degrees of freedom [32] and the third factor is the phase separation, typically involving ferromagnetic metallic and antiferromagnetic charge and orbital ordered insulating domains, leading to nanometer scale coexisting clusters [33]. However, Ru doped $La_{0.7}Pb_{0.3}Mn_{1-x}Ru_xO_3$ bulk samples show an increase in resistance for $T < 0.5T_C$ due to the charge carrier localization (spin canting) which sets in a random magnetic potential [10]. In the case of $La_{1-x}Sr_xMnO_3$ ($x \sim 1/8$), positive MR arises below 165 K attributed to the orbital ordering, which is quite different from the currently studied composition wherein we have found positive MR only <50 K and steady increase in negative MR from 50 to 300 K [32]. However, Hong *et al* have shown positive MR in $La_{0.7}Ba_{0.1}Ca_{0.2}Mn_{0.9}Ru_{0.1}O_3$ thin films due to the coexistence of the antiferromagnetic metallic (AFM), ferromagnetic metallic (FM), and antiferromagnetic insulating (AFI) states. They also showed that the magnetic field induced insulating state in the antiferromagnetic metallic states induces positive MR [34]. In $La_{1-x}Pb_xMn_{0.8}Ru_{0.2}O_3$ ($0.2 \leqslant x \leqslant 0.4$) films antiferromagnetic interactions (suggested by the Goodenough–Kanamori–Anderson (GKA) rule—similar ions couple antiferromagnetically and different ions couple ferromagnetically) due to different redox pairs namely Mn^{4+}–Mn^{4+}, Ru^{4+}–Ru^{4+} and Mn^{3+}–Mn^{3+} cannot be excluded at low temperatures [21, 22].

5. Conclusions

We have reported the effect of Ru–Mn redox interactions on the structural, transport, and magneto-transport properties of pulsed electron deposited $La_{1-x}Pb_xMn_{0.8}Ru_{0.2}O_3$ ($0.2 \leqslant x \leqslant 0.4$) thin films with varying hole carrier density. The structural and microscopic data confirm the epitaxial growth of the films and Ru substitution at Mn sites. 20% Pb doped $La_{0.8}Pb_{0.2}Mn_{0.8}Ru_{0.2}O_3$ thin film shows $T_{MIT} \sim 250$ K despite 20% Ru doping due to the hole carrier mediation in the presence of Mn^{+3}/Ru^{5+} and Mn^{3+}/Mn^{4+} redox couples. Further, 20% Ru substituted films show higher MR than $La_{0.6}Pb_{0.4}MnO_3$ at 310 K, and positive MR at 20 K, due to Coulombic interactions, sustains an applied field up to 5 T in $La_{0.7}Pb_{0.3}Mn_{0.8}Ru_{0.2}O_3$ thin film.

Acknowledgments

Financial assistance from the Defense Research and Development Organization (DRDO), Government of India, INDIA and IIT K (Project No. *DRDO/ERIP/0200187/M/01*) is acknowledged. Brajendra Singh thanks CSIR INDIA for the award of senior research fellowship. We acknowledge the use of the TEM in the NISP laboratory at the University of Maryland, a shared experimental facility of MRSEC (grant No. DMR 0520471).

References

[1] Jin S, Tiefel T H, McCormack M, Fastnacht R A, Ramesh R and Chen L H 1994 *Science* **264** 413
Coey J M D, Viret M and von Molnàr S 1999 *Adv. Phys.* **48** 167
Raveau B, Hervieu M, Maignan A and Martin C 2001 *J. Mater. Chem.* **11** 29
[2] Janker G and Santen V J 1950 *Physica* **16** 337
Janker G and Santen V J 1956 *Physica* **22** 707
[3] Hwang H Y, Cheong S-W, Radelli R G, Marezio M and Batlogg B 1995 *Phys. Rev. Lett.* **75** 914
[4] Zener C 1951 *Phys. Rev.* **82** 403
Zener C 1951 *Phys. Rev.* **81** 440
[5] Damay F, Maignan A, Martin C and Raveau B 1997 *J. Appl. Phys.* **81** 1372
[6] Gupta A, Gong G Q, Xiao G, Duncombe P R, Lecoeur P, Trouilloud P, Wang Y Y, Dravid V P and Sun J Z 1996 *Phys. Rev.* B **54** R15629
[7] Ju H L, Kwon C, Li Q, Greene R L and Venkatesana T 1994 *Appl. Phys. Lett.* **64** 2108
[8] Helmholt R V, Wecker J, Holzapfel B, Schultz L and Samwer K 1993 *Phys. Rev. Lett.* **71** 2331
Trukhanov S V 2003 *J. Mater. Chem.* **13** 347
[9] Manoharan S S, Vasanthacharya N Y, Hegde M S, Satyalakshmi K M, Prasad V and Subramanyam S V 1994 *J. Appl. Phys.* **76** 3923
Leung L K, Morrish A H and Searle C W 1967 *Can. J. Phys.* **47** 2697
[10] Manoharan S S, Sahu R K, Rao M L, Elephant D and Schneider C M 2002 *Eur. Phys. Lett.* **59** 451
Teresa J M De, Ibarra M R, Garcia J, Blasco J, Ritter C, Algarabel P A, Marquina C and Moral D 1996 *Phys. Rev. Lett.* **76** 3392
[11] Vanitha P V, Singh R S, Natarajan S and Rao C N R 1999 *Solid State Commun.* **109** 135
Vanitha P V, Arulraj A, Raju A R and Rao C N R 1999 *C. R. Acad. Sci. Paris* **2** 595
[12] Maignan A, Martin C, Hervieu M and Raveau B 2001 *J. Appl. Phys.* **89** 500
[13] Manoharan S S, Singh B, Driscoll J, Branford W, Cohen L and Besmehn A 2005 *J. Appl. Phys.* **97** 10A304
Malavasi L, Mozzati M C, Tealdi C, Pascarelli M R, Azzonib C B and Flora G 2004 *Chem. Commun.* 1408
[14] Manoharan S S, Singh B and Sahu R K 2007 *J. Appl. Phys.* **101** 09G516
[15] Singh B, Sahu R K, Manoharan S S, Doerr K and Mueller K H 2004 *J. Magn. Magn. Mater.* **273** 358
[16] Sahu R K, Hu Z, Rao M L, Manoharan S S, Schmidt T, Richter B, Knupfer M, Golden M, Fink J and Schneider C M 2002 *Phys. Rev.* B **66** 144415

[17] Strikovski M and Harshavardhan K S 2003 *Appl. Phys. Lett.* **82** 853
[18] Christen H M, Lee D F, List F A, Cook S W, Leonard K J, Heatherly L, Martin P M, Paranthaman M, Goyal A and Rouleau C M 2005 *Supercond. Sci. Technol.* **18** 1168
[19] Choudhary R J, Ogale S B, Shinde S R, Kulkarni V N, Venakatesan T, Harshavardhan K S, Strikovski M and Hannoyer B 2004 *Appl. Phys. Lett.* **84** 1483
[20] Singh B, Manoharan S S, Rao M L and Pai S P 2004 *Phys. Chem. Chem. Phys.* **6** 4199
Wiedenhorst B, Hofener C, Lu Y, Klein J, Alff L, Gross R, Freitag B H and Madar W 1999 *Appl. Phys. Lett.* **74** 3626
[21] Goodenough J B 1955 *Phys. Rev.* **100** 564
Goodenough J B 1958 *J. Phys. Chem. Solids* **6** 287
[22] Kanamori J 1959 *J. Phys. Chem. Solids* **10** 87
[23] Urushibara A, Moritomo Y, Arima T, Asamitsu A, Kido G and Tokura Y 1995 *Phys. Rev.* B **51** 14103
[24] Chakraborty S and Majumdar A K 1996 *Phys. Rev.* B **53** 6235
[25] Schifffer P, Ramirez A P, Bao W and Cheong S W 1995 *Phys. Rev. Lett.* **75** 3336
[26] Lakshmi L S, Sridharan V, Natarajan D V, Rawat R, Chandra S, Sastry V S and Radhakrishnan T S 2004 *J. Magn. Magn. Mater.* **279** 41
[27] Manyala N, Sidis Y, DiTusa T F, Aeppli G, Young D P and Fisk Z 2000 *Nature* **404** 581
[28] Chen P, Xing D Y and Du Y W 2001 *Phys. Rev.* B **64** 104402
[29] Sahu R K, Mohammad Q, Rao M L, Nigam A K and Manoharan S S 2002 *Appl. Phys. Lett.* **80** 88
[30] Manoharan S S, Singh B, Driscoll J, Bradford W, Cohen L and Besmehn A 2005 *J. Appl. Phys.* **97** 10A304
[31] Coey J M D, Viret M, Ranno L and Ounadjela K 1995 *Phys. Rev. Lett.* **75** 3910
[32] Nojiri H, Kaneko K, Motokawa M, Hirota K, Endoh Y and Takahashi K 1999 *Phys. Rev.* B **60** 4142
[33] Dogotto E, Hotta T and Moreo A 2001 *Phys. Rep.* **344** 1
[34] Hong N H, Sakai J, Nouden J G, Gervais F and Gervais M 2004 *Phys. Rev.* B **67** 134412